# UTILIZATION OF DIFFERENT SENSORS IN UAV FOR THE DETECTION AND OPTIMAL VISUAL OBSERVATION OF THE MARKS OVER BURIED ANCIENT REMAINS

**Dimitris Kaimaris**

*School of Spatial Planning and Development (Eng.),*
*Aristotle University of Thessaloniki, Thessaloniki, Greece*
*(kaimaris@auth.gr)*

**ABSTRACT**

The utilization of a variety of data from Aerial and Remote Sensing Archaeology (aerial photographs, satellite images, multispectral, thermal images, and lidar data from Unmanned Aerial Vehicle-UAV, Google Earth images, etc.), aids to identify ancient remains. In present investigation elements of main features visible as crop marks of covered ancient building structures are studied in two locations in Northern Greece; north of ancient Amphipolis and the second within the walls of the ancient city of Philippi. The work focuses mainly on the various data collected with the UAV and their processing, aiming at the visual improvement and optimal observation of the marks, with results explored via archive data from aerial and Remote Sensing Archaeology. Regarding UAV image capturing, a sensor sensitive to the visible area of the spectrum (digital DSLR camera) was used in the first location, while a multispectral (Parrot Sequoia) and thermal (Flir Vue Pro) sensor was additionally used in the second location. In addition to the geometric correction of all images in both locations, in Philippi, vegetation index maps were created utilizing the bands of the multispectral sensor that was placed in the UAV. The marks in the Amphipolis are captured with the highest spatial resolution in the UAV images. In Philippi the marks are optimally located visually and have a high observation intensity in the Near-infrared (NIR) image of the multispectral sensor and in the maps of Simple Ratio (SR) and Green chlorophyll index (GCI).

# 1. INTRODUCTION

The wider region of Eastern Macedonia (Northern Greece), from ancient Amphipolis to Philippi (fig. 1), has been studied for the last 20 years with the help of Aerial and Remote Sensing Archaeology, to locate marks of covered ancient remains. The marks of the covered Via Egnatia with a total length of about 55Km and the archaeological discovery (by archaeological excavation) of its parts, as well as the location of hundreds of other nearby covered possible ancient remains have been successfully identified (Georgoula et al., 2003; Kaimaris, 2006; Kaimaris et al., 2011; Kaimaris et al., 2012; Kaimaris and Patias, 2015).
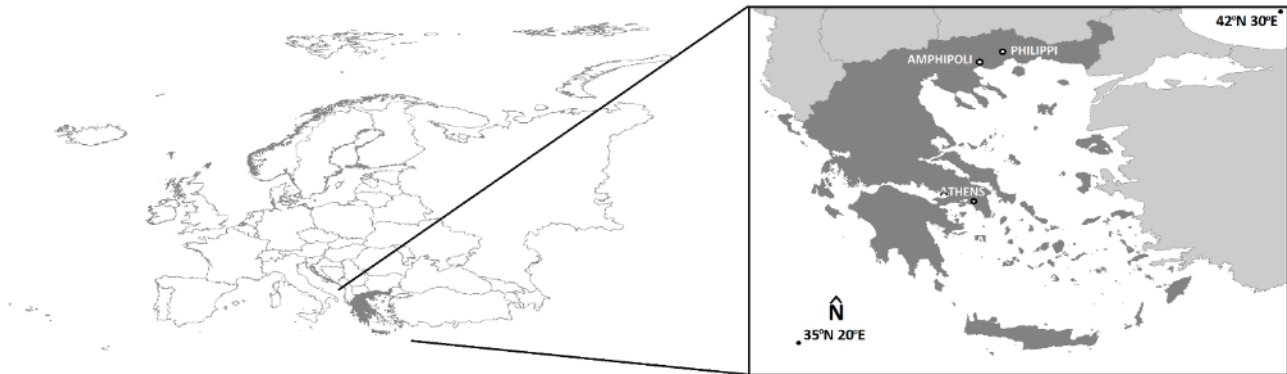


*Figure 1. Greece in the European continent and Aphipolis and Phillipi location in Greece*

The ancient city of Amphipolis is built in the place of the Thracian tribe of Idonon's older settlement ("Nine Roads"), close to the delta of the Strimona River (Kaimaris et al., 2016). The settlement is reported by Thucydides (Jones, 1970), Stravonas (Baladie, 1989), and Herodotus (Godley, 1921). Its location was a strategic and economic node. The Parians, after fierce battles with the Thracians, they started building fortified cities in the vicinity of "Nine Roads", such as Galipsos, Oistimi, Neapolis (Kavala), Strimi (Lazaridis, 1993). Thrace and Eastern Macedonia were temporarily conquered by Persians during the expedition of King Darius to South Greece. Following the defeat of the Persians, Thasos became a member of the first Athenian Alliance in 477 B.C. The Spartan general Vrasidas occupied the city of Amphipolis in 424 B.C. (Jones, 1970). In 358–357 B.C., Philippos II occupied Amphipolis (Lazaridis, 1993). During the Hellenistic era-up to the battle of Pidna in 168 B.C., when the Romans occupied the state of Macedonia-Amphipolis was the center of exploitation of all the mines in the area, an important commercial center, one of the most powerful royal mints of Macedonians, a powerful fortress of great military importance, and a naval base of Alexander the Great, from which his fleet started the expedition to the East (Goukowsky, 1978). Following the conquest of Macedonia by the Romans, Macedonia was divided into four administrative regions. Amphipolis (conquered by Aemilius Paullus) was the capital city of the first region (Baladie, 1989).

The first historical evidence for the existence of organized life in the area of Philippi, dates back to prehistoric times. Residents of the island of Thassos, led by the exiled Athenian politician Kallistratos, founded the colony of Krinides (the first name of Philippi) in 360 B.C. In 356 B.C. the settlers, in the face of the threat of the local tribes of Thrace, sought the help of the rising force of Hellenism, the king of Macedonia Philip II, who captured it, fortified it and installed Macedonian citizens, renaming it to Philippi. Philip II turned Philippi to a significant economic power of the kingdom, with the discovery and intensive exploitation of new gold mines. In the time of the Roman Republic, the great Roman road, Via Egnatia, that crossed Philippi, brought the city back to the forefront of great historical events. A milestone in the history of Philippi is the great battle outside the western walls of the city in 42 B.C., between two Roman armies, the Democrats led by Brutus and Cassius, and the successors of the policy of Julius Caesar led by Octavian and Antonios. The defeat of the Democrats at the Battle of Philippi gave Octavian the opportunity to lead the Roman Empire. The city was transformed into a Roman colony, with the settlement of Roman settlers, veterans of the Roman army and flourished in the 2nd century A.D. In 49/50 A.D. the Apostle Paul arrived at the city and founded the first Christian church in Europe. At the end of the 6th and the beginning of the 7th century A.D. the city showed signs of severe decline, as it was not able to restore the late Roman and early Christian buildings, which began to be destroyed by earthquakes, nor to erect new ones (Kaimaris, 2002).

The "reflection" of a buried structure in the ground or vegetation, captured in the analog or digital image, is the result of the phenomenon of the interaction of the buried monument with the above elements. This

" reflection" is internationally called "Mark". A buried monument can be a "compact construction" (such as the boundaries of a building), or an "open construction" (such as an ancient trench). The effect of a buried monument on the soil or the crop results in the appearance of marks (crop or/and soil marks). The categories of marks and their intensity depend on a series of factors, such as the type, size and depth of the buried monument, the quantity of ground humidity, the air temperature, the ground and the upper ground type, the vegetation type, the period and intensity of rainfall and so on. These factors cause differing ground humidity and temperature, plus variances in quality (height, density, colour) and temperature of the vegetation, not only in the material that covers the monument, but also in the material surrounding the monument (Betti, 1964; Ciminale and Ricchetti, 1999; Wilson, 1982; Riley, 1987). Thus, the quantity of electromagnetic energy that is reflected or emitted from the ground or the vegetation is different, and this is recorded by the sensors, allowing observation of the buried construction's marks in the images (Kaimaris, 2006).

Regarding the optimal imaging period for marks detection, methodological procedures have been developed and allow, through different observations in time, the documentation of the theoretically best period and / or the reduction of the range of the best period for marks detection (Kaimaris, 2006; Kaimaris et al., 2012; Kaimaris and Patias, 2015; Fagan, 1959; Betti, 1963; Jones and Evans, 1975; Wilson, 1982; Brooks and Johannes, 1990; Barrett, 1993; Ciminale and Ricchetti, 1999; Hanson and Olten, 2003; Challis et al., 2009). In the wider study area, the optimal period for the detection of marks is from mid-April to mid-May (Kaimaris, 2006; Kaimaris et al., 2012; Kaimaris and Patias, 2015). In Kaimaris et al (2015) the identification of the optimal imaging period for marks detection was attempted. In this paper we successfully utilize the above results for taking shots within the optimal imaging period.

In fact in the context of the control of the continuous preservation of the existing known marks in the wider area (from Amphipolis up to Philippi), but also of the study of the localization of new marks, new and unknown up to date marks of possible covered archaeological structures have been discovered. Therefore, the aim of this paper is the presentation of an unknown possible archaeological site with marks of covered possible building structures north of Amphipolis, at a distance of about 18Km from the ancient city.

Black and white (BW) intertemporal aerial photographs, panchromatic (PAN) and multispectral (MS) satellite imagery, images from Google Earth (GE) and optical imagery from Unmanned Aerial Vehicle (UAV) are utilized. Also, in well-known archaeological site, are presented marks of unknown possible ancient buildings, within the walls of the ancient city of Philippi. Images from Google Earth and optical, MS and thermal images from UAV are used. In this site an attempt is made to utilize already known remote sensing indexes, for the visual improvement of the marks.

## 2. UAV AND SENSORS

UAV was used in both study areas. Six propellers make the coordinate movement possible. The UAv flight is conducted either automatically or controlled manually via remote control. The batteries, electronic boards, avionics processors, 3 cameras (digital DSLR camera, MS and thermal camera, Table. 1) and sensors (Inertial Measurement Unit-IMU, GPS, gyroscope, accelerometer and barometer) are placed in the central axis of the UAV's body. It must be mentioned that at the time of the image capturing at the north of Amphipolis, only the digital DSLR camera (Table 1) was available. As far as the flight plan is concerned, the ground station enables its programming. Cameras rotate vertically by 180 degrees (± 90 degrees from nadir) on the gimbal. The autopilot Wookong M of DJI, which includes a Controller, an IMU, and a GPS, is used on the UAV. The accuracy of the horizontal axis reaches approximately ±2 m, of the vertical axis ±0.5 m and of the angle measurement (IMU) in the three axes (X, Y, Z) ranges from approximately 1 to 2 degrees (according to the specifications of the autopilot).

UgCS© software is used for flight planning and stereoscopic image coverage. During the flight the autopilot gives the command to take images and records the shooting positions ($\varphi$, $\lambda$ and H) in the World Geodetic System 1984 (WGS84). The lifting capacity of the UAV is 2.5 kg, and the flight time ranges between 10 and 15 min (Kaimaris et al., 2018a). In addition to the above, the UAV is a self-made construction, i.e. it was not purchased at its present form, but the supply of its individual parts firstly took place. In order to fly safely and prevent serious accidents from falling, a UAV parachute has been added to ensure smooth and safe landing on the ground. The parachute launches by a stand-alone remote controller (Skycat, 2014).

*Table 1. The characteristics of the cameras of the UAV*

| Camera | Technical specifications |
|---|---|
| DSLR Canon 1200D | CMOS sensor 22.3 mm x 14.9 mm, 18 MP, Canon lens EF-S 17–85 mm f/4–5.6 IS USM, focal length 17-85 mm and diaphragm opening range 4-5.6 |
| Sequoia (Parrot) | Multispectral camera (Body): <br> • 4 spectral cameras: Green 530-570 nm, Red 640-680 nm, Red Edge 730-740 nm, Near Infrared 770-810 nm, 1.2 MP, 10 bits Global shutter. Pixel Size / Focal Length / Pixel count: 3.75 μm / 3.98 mm / 1280x960. <br> • RGB Camera 16 MP Rolling shutter. Pixel Size / Focal Length / Pixel count: 1.34 μm / 4.88 mm / 4608 × 34560. <br> • IMU + Magnetometer <br> • 72g <br> Sunshine sensor: <br> • 4 spectral sensors with the same filters as those of the Multispectral camera (Body). <br> • GPS. <br> • Inertial Measurement Unit (IMU) and Magnetometer <br> • 35g |
| Flir Vue Pro | Resolution 640×512, Lens 19 mm; 32° x 26°, Spectral Band 7.5 - 13.5 μm, Full Frame Rates 30 Hz |

The installation of multispectral or/and thermal sensors on UAV is an ideal solution to address the drawbacks of satellite systems in collecting data (Berni et al., 2009). UAV (multi-propeller, fixed wing, modeling helicopters, etc.), with multispectral or/and thermal sensors (such as Sequoia and Flir Vue Pro), have the ability to collect multispectral or/ and thermal images at a lower cost compared to satellites. These sensors produce images of very small pixel size on the ground, at the level of centimeters, that is, with much better spatial resolution in comparison with the captured images from satellite platforms (Candiago et al., 2015). However, UAV are significantly disadvantaged compared to satellite systems, as far as the surface area they can capture. The flight height and time, the lifting load but also the platform type (e.g. multi-propeller, fixed wing etc.) are the major limitation factors, leading to small captured areas against the satellite images.

## 3. METHODS AND RESULTS

### 3.1. *The site north of Amphipolis: Archive data, new data and their processing*

About 18 Km north of Amphipolis (40° 58'50.16 "N, 23° 55 ' 33.67 "E), in the satellite image QuickBird-2 with date of capturing 02/05/2005 (Fig. 2.cf, Tab. 2), within the best period for marks detection, linear crop marks are detected (Fig. 2. f). The geometric image correction in the Greek Geodetic Reference System 1987 (GGRS87) was performed in the Erdas Imagine© software (utilizing 36 Ground Control Points/GCPs, 1m horizontal accuracy and 2m altitude accuracy,

known Geometric Sensor Model derived from the image, Digital Terrain Model/DTM, Tab. 2 (Henrico and Combrinck, 2016; Krishnana et al., 2016; Kaimaris, 2018b; Hatzopoulos et al., 2017; Liritzis et al., 2015) and during the geometric correction the Root Mean Square Error/RMSE was 5.4m and the spatial resolution of the generated upright satellite image was 0.6m).

The corresponding image was collected from Google Earth (Fig. 2.a, b and Fig. 3.c), which, although spatially and spectrally degraded (Kaimaris et al., 2011), allows the observation of marks with low visual intensity.

Intertemporal aerial photographs and additional images from Google Earth were collected in the same study area (Tab. 2). The aerial photographs' capturing period is unknown, they were digitized at 1200dpi, while for their geometric correction in GGRS87 the Erdas Imagine© software was used (known internal orientation elements, the central projection model, 18 GCPs horizontal accuracy of 1m and height of 2m, known DTM, Tab. 2, and the RMSE of the aerial photographs of 1945 was 8.0m and spatial resolution of the ortho image is 0.9m, of the aerial photographs of 1953 was 1.4m and spatial resolution of the ortho image is 0.2m (Kaimaris et al., 2019)). For the geometric correction of the Google Earth images (Tab. 2 and Fig. 3.c-p) in GGRS87 the same software was used (affine transformations were performed by selecting 8 to 10 corresponding points with the ortho satellite image QuickBird-2 of 2005 and the RMSE ranged between 1-2m and spatial analysis of the corrected images reached 1m).
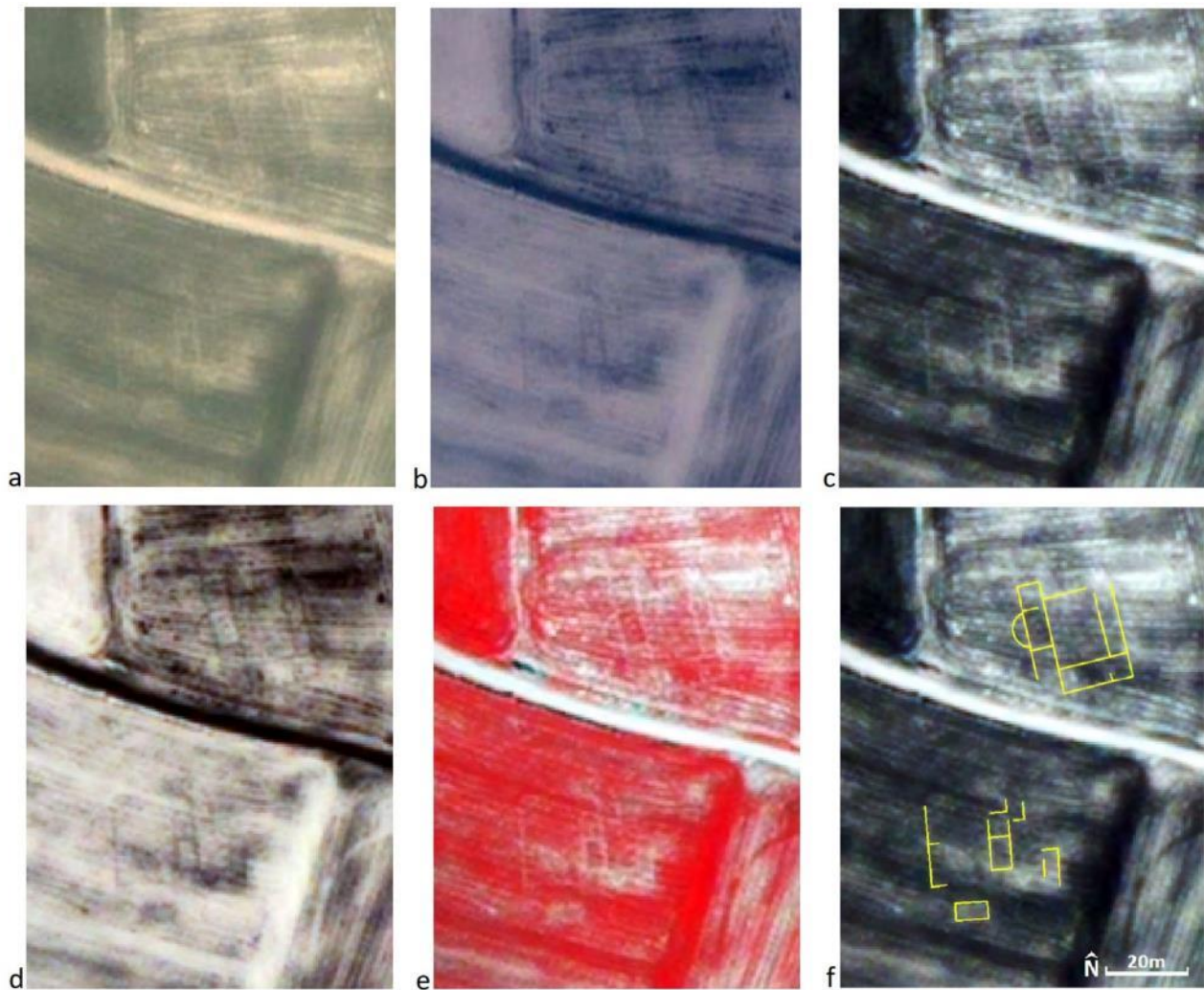
*Figure 2. North of Amphipolis; a. Image from Google Earth (GE) with date of capturing 02/05/2002 at the study area (40°58'50.16 "N, 23°55'33.67" E); b. The negative of image a; c. The original QuickBird-2 satellite image (Red, Green, Blue) with date of capturing 02/05/2005; d. The negative of image c; e. The QuickBird-2 satellite image (Near-infrared / NIR, Green, Blue) and f. Presentation of crop marks in yellow*

*Table 2. Archive data: Location of site at the north of Amphipolis*

| Data | Information |
|---|---|
| Digital Terrain Model (personal data) | • Point Grid: 5x5m<br>• Horizontal accuracy: 0.5m<br>• Vertical accuracy: 2m |
| Satellite image (personal data) | • QuickBird-2<br>• Date: 2/5/2005<br>• Panchromatic, Spatial resolution: 0.6m<br>• Multispectral (Red/R, Green/G, Blue/B, Near-infrared/NIR), Spatial resolution: 2.4 m<br>• Pansharpen (R,G,B,NIR), Spatial resolution: 0.6 m |
| Ground Control Points (National Cadaster, 2021) | • X, Y horizontal accuracy: 1m<br>• Z from DTM |
| Google Earth images | • Dates: 2/5/2005, 21/3/2010, 26/3/2010, 20/3/2012, 18/3/2014, 1/10/2014, 30/5/2016, 20/10/2017, 24/8/2018, 16/9/2018<br>• True color |
| Aerial Photographs (personal data) | • Date: 1945 (only year), Scale: 1:42,000, Black and White (BW), Spatial resolution: 0.9m<br>• Date: 1953 (only year), Scale: 1:10,000, BW, Spatial resolution: 0.2m |
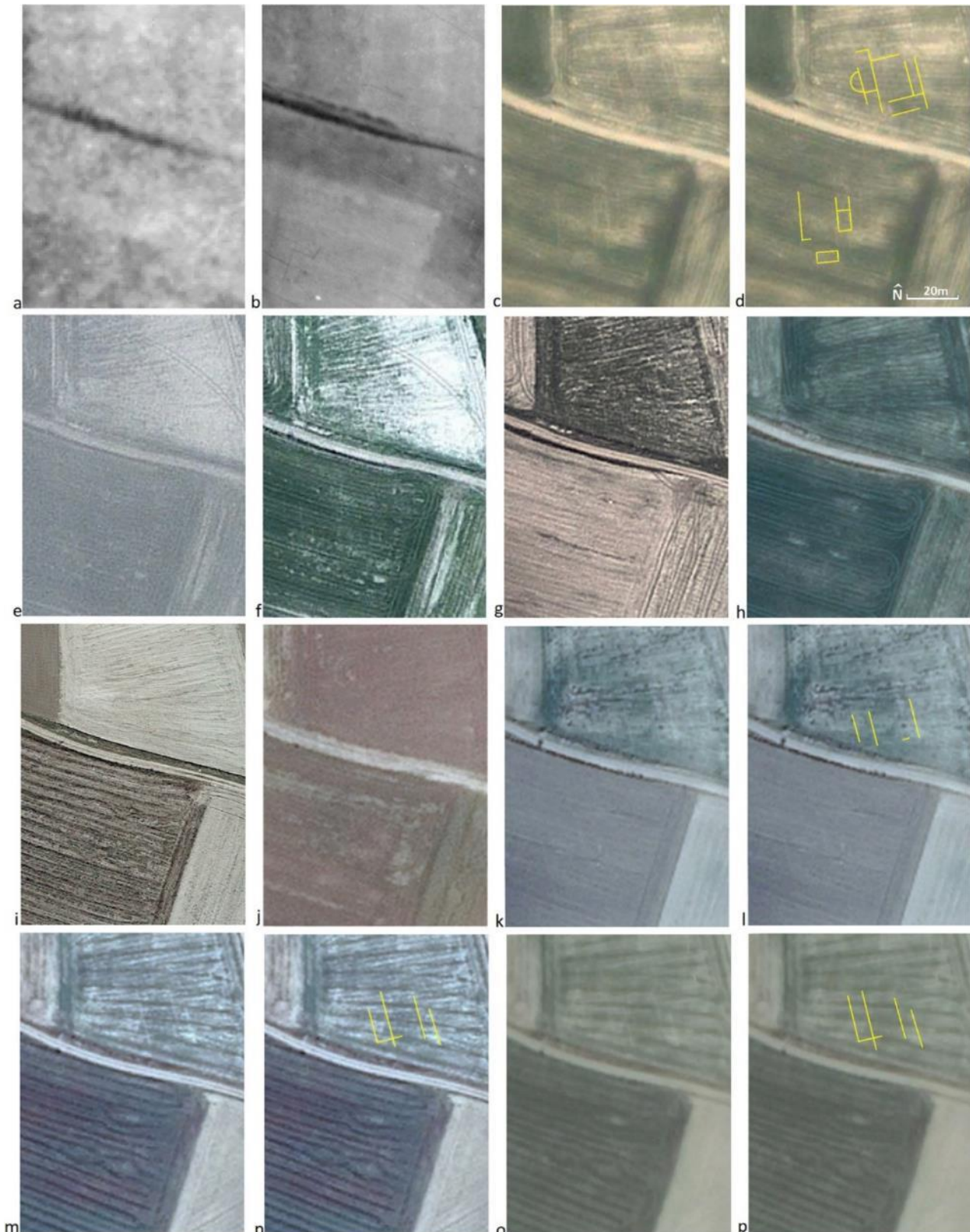
*Figure 3. North of Amphipolis; a. Aerial photograph of 1945; b. aerial photograph of 1953; c. image of Google Earth (GE) 2/5/2005; d. demarcation of crop marks of the image of GE 2/5/2005 in yellow; e. GE 21/3/2010; f. GE 26/3/2010; g. GE 20/3/2012; h. GE 18/3/2014; i. GE 1/10/2014; j. GE 30/5/2016; k. GE 20/10/2017; l. the design of the marks of the image of GE 20/10/2017 in yellow; m. GE 24/8/2018; n. the design of the marks of the image of GE 24/8/2018 in yellow; o. GE 16/9/2018; p. the design of the marks of the image of GE 16/9/2018 in yellow*

The UAV image capturing (which only used the digital DSLR camera) at the study area north of Amphipolis took place on 10/5/2019 (01:17 p.m.), ie within the optimal period for marks detection. The flight altitude was 50m and the autopilot conducted the flight covering the study area with 6 strips and image overlap of 80% forward and side. 94 images were collected (Red, Green, Blue), to which the coordinates of the receiving centers were subsequently added (data in WGS84 recorded in the UAV autopilot). As the high spatial accuracy of the final products

(eg DTM, ortho image) was not the main goal, but a relative spatial accuracy in GGRS87, no additional information, such as GCPs, was used to produce the ortho image. The utilized software was Agisoft Metashape©, in which through the use of the coordinates of the images' capture centers, the production and the automatic transformation (convert) of the coordinate systems (from WGS84 to GGRS87) of the ortho image (Fig. 4, spatial resolution 1.2cm) is allowed.
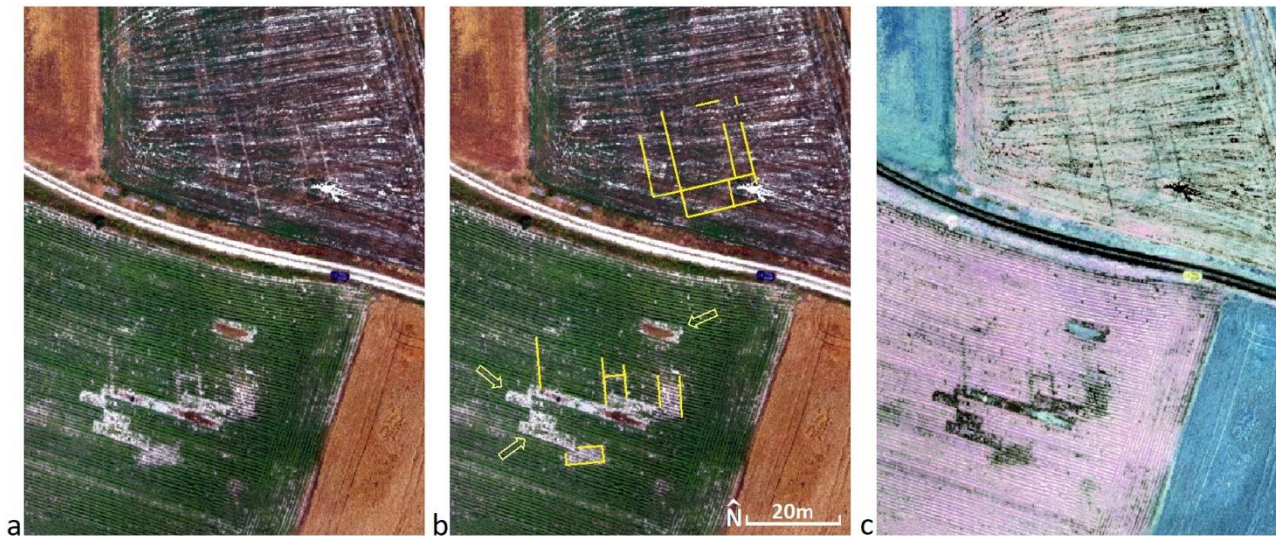


*Figure 4. North of Amphipolis; a. The ortho image of the UAV on 10/5/2019; b. indication of crop marks with yellow lines and positions without any vegetation with yellow arrows; c. the negative of image a*

### 3.2. *The site in Phillipi: Archive data, new data and their processing*

In the archaeological site of Philippi (41° 00'38.2 "N, 24° 17'14.2" E) (Figs. 1 and 5), from the existing visible archaeological remains (theater, basilicas, market, etc., shown in the center of Fig. 5) up to the wall of the ancient city (pointed with yellow arrows in Fig. 5), the presence of covered ancient remains is probable).

In an area (random selection) within the walls of Philippi (in a yellow frame in Fig. 5) images from Google Earth were collected (Tab. 3 and Fig. 6). Erdas Imagine© software was used for the geometric correction of google earth images in GGRS87 and affine transformations were performed using 8 to 10 GCPs (1m horizontal accuracy and 2m altitude accuracy, Tab. 3) (the RMSE ranged between 1-2m and the spatial resolution of ortho images was 1m).
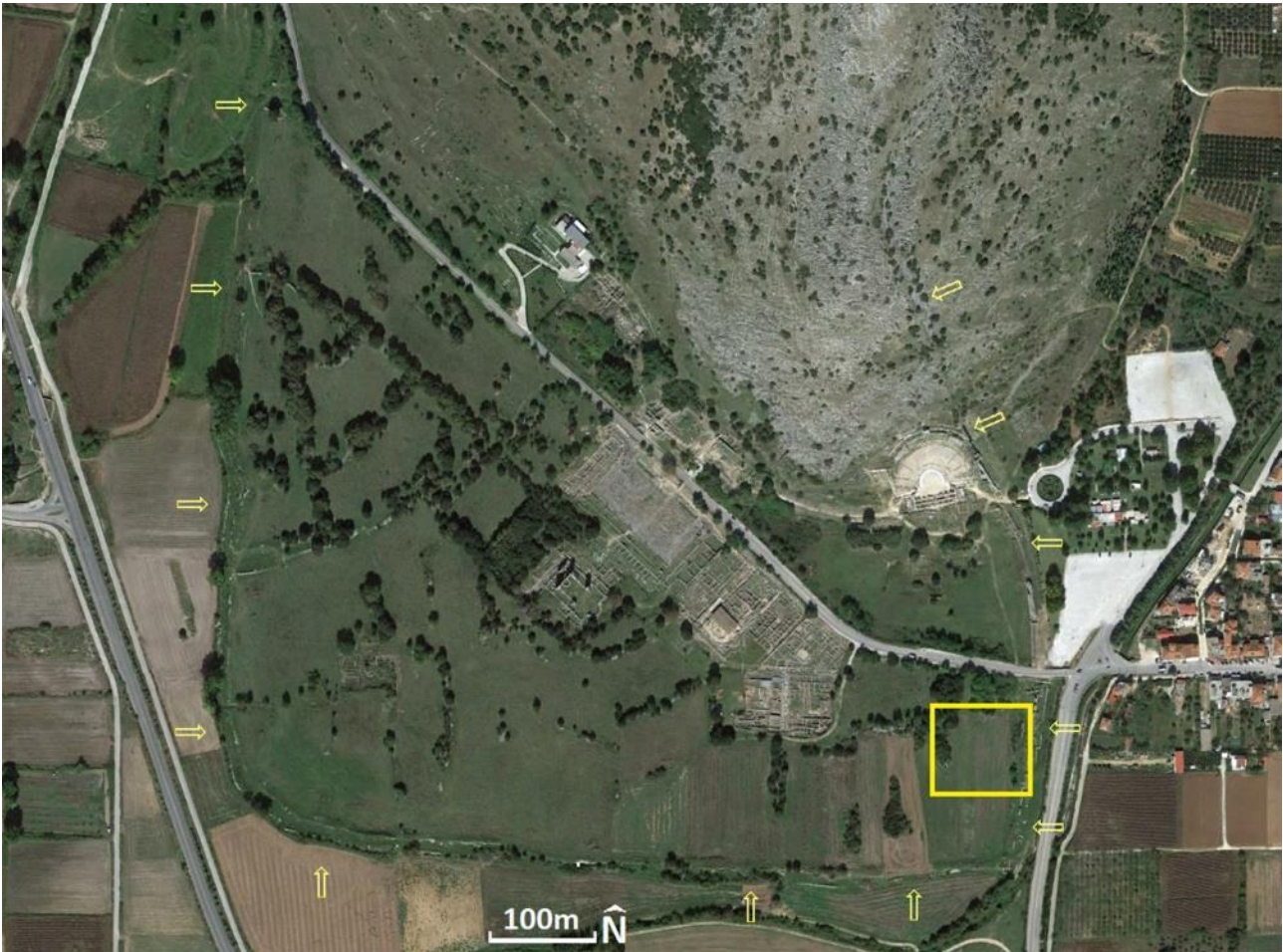
*Figure 5. The ancient city of Philippi (from Google Earth, date 01/10/2014). The ancient wall pointed with yellow arrows and the area of the collection of images for the identification of marks in a yellow frame*

*Table 3. Archive data: Philippi.*

| Data | Information |
| --- | --- |
| Digital Terrain Model (personal data) | • Point Grid: 5x5m<br>• Horizontal accuracy: 0.5m<br>• Vertical accuracy: 2m |
| Google Earth images | • Dates: 10/5/2003, 29/4/2004, 16/11/2010, 9/4/2011, 24/9/2013, 3/11/2013, 1/10/2014, 17/5/2015, 29/10/2016, 20/12/2016, 13/6/2017, 21/11/2017.<br>• True color |
| Ground Control Points (National Cadaster, 2021) | • X, Y horizontal accuracy: 1m<br>• Z from Digital Terrain Model |

*Figure 6. Philippi, the area included in the yellow frame in Fig. 5; Intertemporal images of google earth (GE) in the yellow study area of figure 5; a. GE 10/5/2003; b. GE 29/4/2004; c. GE 16/11/2010; d. GE 9/4/2011; e. GE 24/9/2013; f. GE 3/11/2013; g. GE 1/10/2014; h. GE 17/5/2015; i. GE 29/10/2016; j. GE 20/12/2016; k. GE 13/6/2017 and l. GE 21/11/2017.*

Images were taken at the study area with the UAV on 14/5/2021 (12:55 p.m.), ie within the optimal period for marks detection. Two new sensors were used (besides the digital DSLR camera that the UAV has), the MS and thermal sensor for UAV (Tab.1).

The flight altitude was 50m and the autopilot conducted the flight covering the study area with 4 strips and image overlap 80% forward and 75% side for the digital DSLR camera. In the case of the MS sensor the number of strips, the forward and side overlap is the same as in the case of the digital DSLR camera as, on the one hand the MS sensor covers approximately the same area (75% side overlap, Fig. 7) with the DSLR camera, and on the other hand 80% forward overlap was calculated and introduced with time laps in the MS sensor software. Also, in the case of the thermal sensor, the number of strips is the same as the previous two cases of sensors, the side overlap is 40% (Fig. 7) and the 80% forward overlap was calculated and inserted with time laps by the thermal software sensor.

58 images (Red, Green, Blue) were collected from the digital DSLR camera, to which the coordinates of the receiving centers were subsequently added (data in WGS84 recorded in the UAV autopilot). Similarly,

in the case of the site north of Amphipolis, no additional information, such as GCPs, was used to produce the ortho image. The editing software was Agisoft Metashape©, which uses the coordinates of the images' capture centers to generate and automatically convert the coordinate systems (from WGS84 to HGRS87) of the ortho image (Fig. 8.a, spatial resolution 1.2cm).
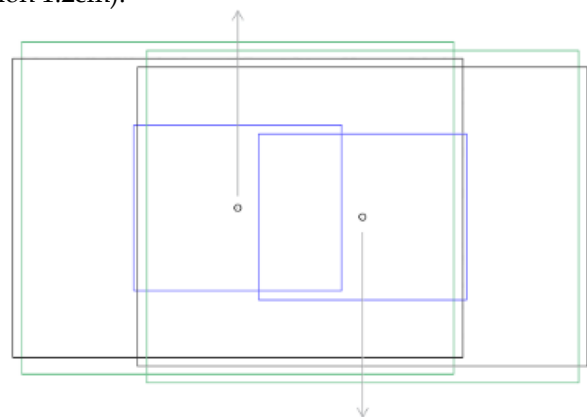


*Figure 7. The overlays between two strips of images from a height of 50m for the digital DSLR camera (with black frame each image, 75% side overlap), the MS sensor (in green, 75% side overlap) and the thermal sensor (in blue, 40% side overlap). In circles the shooting centers and with gray arrows the direction of the two strips*
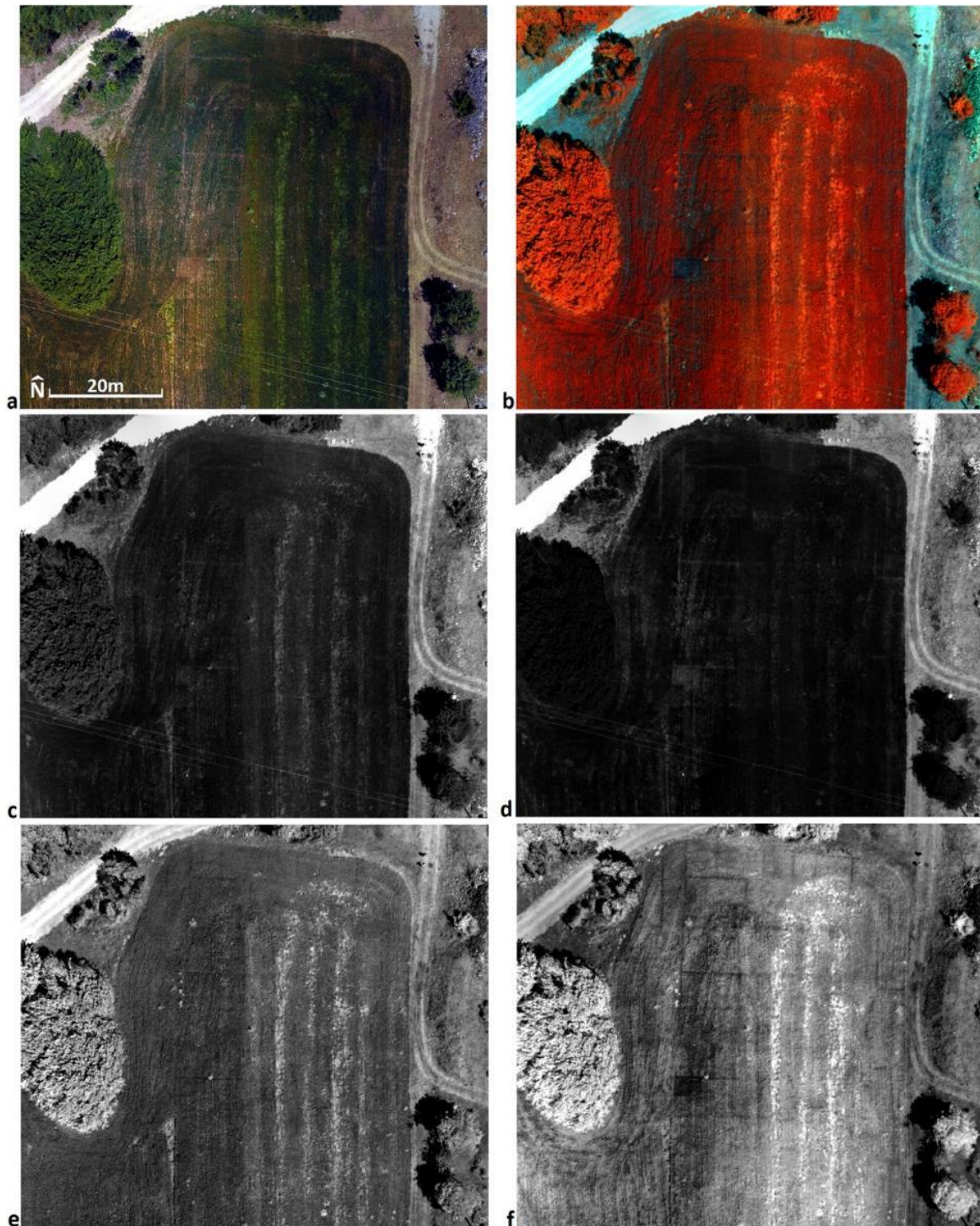
*Figure 8. Philippi, the area included in the yellow frame in Fig. 5; a. The ortho image of the digital DSLR camera; b. The ortho MS image (NIR, Green, Red); c. The ortho Green image of the MS sensor; d. The ortho Red image of the MS sensor; e. The ortho Red Edge image of the MS sensor; f. The ortho NIR image of the MS sensor.*

Despite the fact that the MS sensors which are used on UAVs have progressed as far as their sensor performance is concerned, the data's radiometric quality is still uncertain. Calibration will be necessary as the reliability of spectral information is unclear (Aasen et al., 2018; Borgogno and Gajetti, 2017; Franzini et al. 2019). The calibrations are conducted with the aid of spectral targets. The reflectance response of the spectral targets is calculated in situ with a spectrometer (Franzini et al. 2019; Ahmed et al., 2017; Miyoshi et al., 2018; Guo et al., 2019; Mafanya et al. 2018; Johansen and Raharjo, 2017; Honkavaara and Khoramshahi, 2018). In this paper a spectrometer was not available and therefore shortly before the end of the images the suitable calibration target of the Sequoia sensor was

imaged, whereas with the aid of Agisoft Metashepe© the prescribed radiometric calibration procedure was performed (Franzini et al. 2019; Ahmed et al., 2017; Miyoshi et al., 2018; Guo et al., 2019; Mafanya et al. 2018; Johansen and Raharjo, 2017; Honkavaara and Khoramshahi, 2018; Assmann et al., 2019). Target was automatically detected by the software and the reflectance values of the green, red, red-edge and NIR spectral bands were defined as equal to 0.189, 0.201, 0.227 and 0.260 respectively.

Insufficient quality in the solution position for georeferencing images is observed when the GPS (Global Positioning System) is integrated with the Sequoia. Metric errors have been documented by some authors (Franzini et al. 2019; Assmann et al., 2019; Turner et al., 2012; Chiang et al., 2012; Lussem et al.,

2017). In this paper the relatively accurate correlation of the generated ortho MS images with the rest ortho images of the position of interest was the main goal. Thus, by the utilization of the coordinates of the image capture centers from the GPS of the MS sensor, the production and the automatic transformation (convert) of the coordinate system (from WGS84 to HGRS87) of the ortho images (spatial resolution 5cm, Fig. 8.b.-f) in Agisoft Metashepe© was possible.

Because the marks are visually observed on a crop according to figure 8 (a and b), index maps related to the crop will be created and the possible improvement of their observation will be checked. Thus, the Vegetation Index formulas of Table 4 were created in the same software and the corresponding vegetation index maps were produced (Fig. 9).

*Table 4. List of Vegetation indexes that were used in the site of Philippi.*

| Index | Abbreviation | Formula | Comment |
|---|---|---|---|
| NDVI | Normalised Difference Vegetation Index | $\frac{NIR - Red}{NIR + Red}$ | Normalised ratio ranging for the measurement of green vegetation (Franzini et al. 2019; Rouse et al., 1974) |
| GNDVI | Green Normalised Difference Vegetation Index | $\frac{NIR - Green}{NIR + Green}$ | Modification to NDVI, increased sensitivity to chlorophyll concentration (Franzini et al. 2019; Gitelson et al., 1996) |
| NDVIRE | Red-Edge Normalised Difference Vegetation Index | $\frac{RedEdge - Red}{RedEdge + Red}$ | Modification to NDVI, instead of near infrared (NIR) reflectance, red-edge information was used (Franzini et al. 2019; Gitelson and Merzlyak, 1994) |
| SAVI | Soil adjusted vegetation index | $1.5 * \frac{NIR - Red}{NIR + Red + 0.5}$ | SAVI and NDVI are almost alike in their formulation, with the only difference being that an adjustment factor is used by SAVI so as to minimize the effects of soil on the spectral signal (Huete, 1988). |
| GSAVI | Green soil adjusted vegetation index | $1.5 * \frac{NIR - Green}{NIR + Green + 0.5}$ | The green band instead of the red is used in the calculation of GSAVI, which, at the rest, follows the SAVI formula structure (Peter et al., 2020) |
| SR | Simple Ratio | $\frac{NIR}{Red}$ | Simple vegetation distinction is conducted by Ratio of NIR scattering to chlorophyll absorption (Moriarty et al., 2018) |
| MSR | Modified Simple Ratio | $\frac{\left(\frac{NIR}{Red}\right) - 1}{\sqrt{\left(\frac{NIR}{Red}\right) - 1}}$ | Sensitivity to vegetation characteristics is improved by the combination of renormalized NDVI and SR (Moriarty et al., 2018) |
| GCI | Green chlorophyll index | $\left(\frac{NIR}{Green}\right) - 1$ | The content of leaf chlorophyll in various species of crops is estimated through the index (Peter et al., 2020). |
| GRVI | Green Ratio Vegetation Index | $\frac{NIR}{Green}$ | Simple ratio modification, sensitive to rates of photosynthesis (Moriarty et al., 2018). |
| NDRE | Normalised Difference Red-Edge Index | $\frac{NIR - RedEdge}{NIR + RedEdge}$ | Monitoring chlorophyll content is able through the sensitivity and efficacy of the index (Franzini et al. 2019; Barnes et al., 2000) |
| NGRDI | Normalised Green Red Difference Index | $\frac{Green - Red}{Green + Red}$ | Biomass showed positive correlation to the index (Franzini et al. 2019; Gitelson et al., 2002; Hunt et al., 2005) |
| NLI | Nonlinear Vegetation Index | $\frac{NIR * NIR - Red}{NIR * NIR + Red}$ | Linear relationships with vegetation parameters were emphasized by the modification to NDVI (Moriarty et al., 2018) |
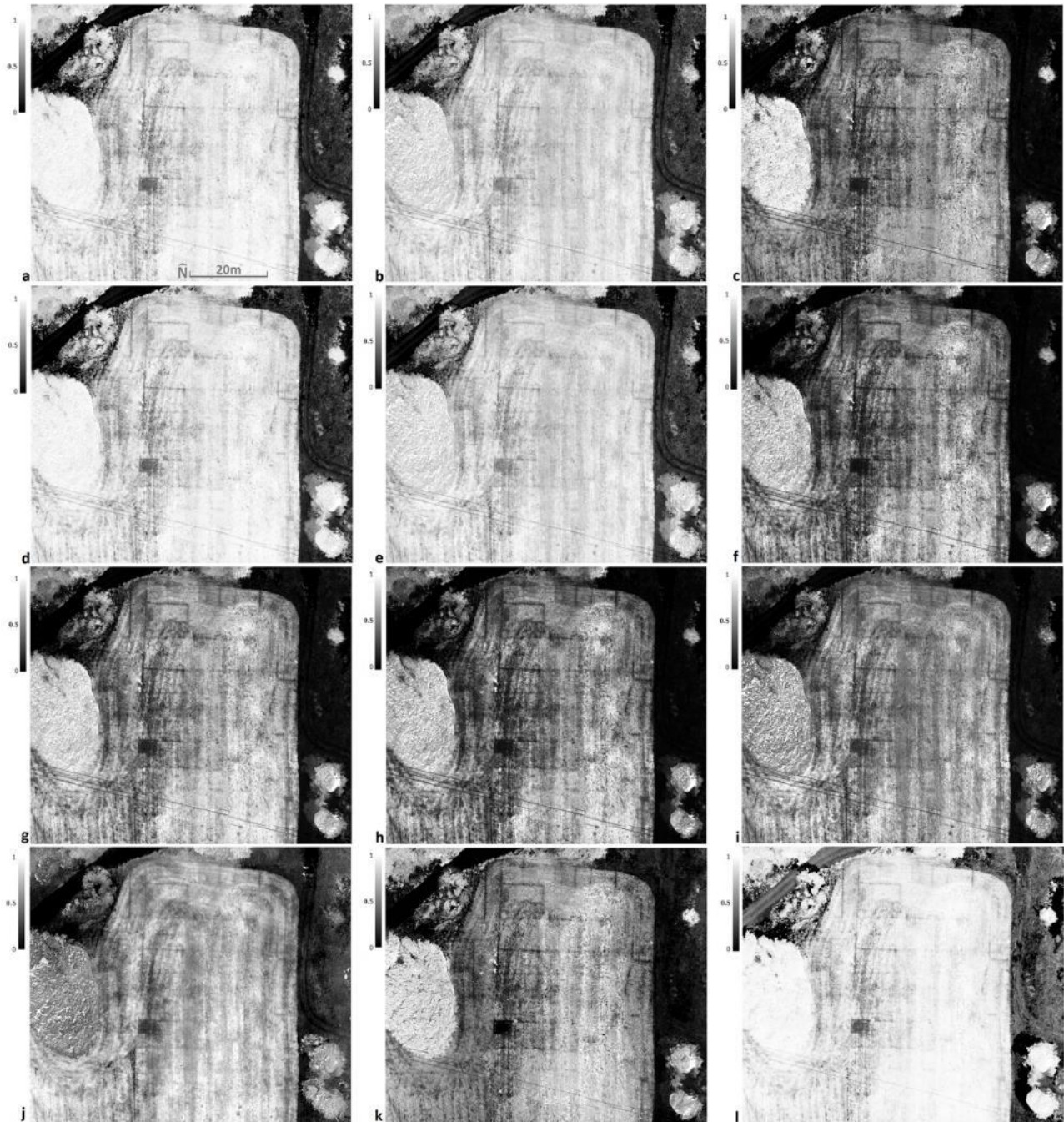
*Figure 9. Philippi, the area included in the yellow frame in Fig. 5; The grayscale of the images is from 0 (black) to 1 (white), giving 0 to the less good and 1 to the best result of the index (eg for NDVI the value 0 corresponds to pixels without crop, the value 0.5 to pixels with poor growth or with poor crop health and the value of 1 to pixels with good growth or healthy crop); a. NDVI; b. GNDVI; c. NDVIRE; d. SAVI; e. GSAVI; f. SR; g. MSR; h. GCI; i. GRVI; j. NDRE; k. NENTI; l. NLI.*

In the case of the thermal sensor, its images take up less space than those of the digital DSLR camera and the MS sensor (Fig. 7). Images 47 were taken (12:55 p.m.), while the sensor does not have GPS. In this case, the Agisoft Metashape© software performed image alignment, clouds and geometrically corrected image generation in an arbitrary coordinate system. Afterwards, in Erdas Imagine© software an affine transformation was conducted through the selection of 12 corresponding points from the ortho NIR image of the MS sensor (RMSE was approximately 5cm and spatial resolution of the geometrically corrected image 4cm in GGRS87). Finally, the sensor does not automatically calculate the temperatures of objects on the earth's surface, and for this reason figure 10.a shows white to black tones of gray, the pixels with the warmest to the coldest objects on the earth's surface.
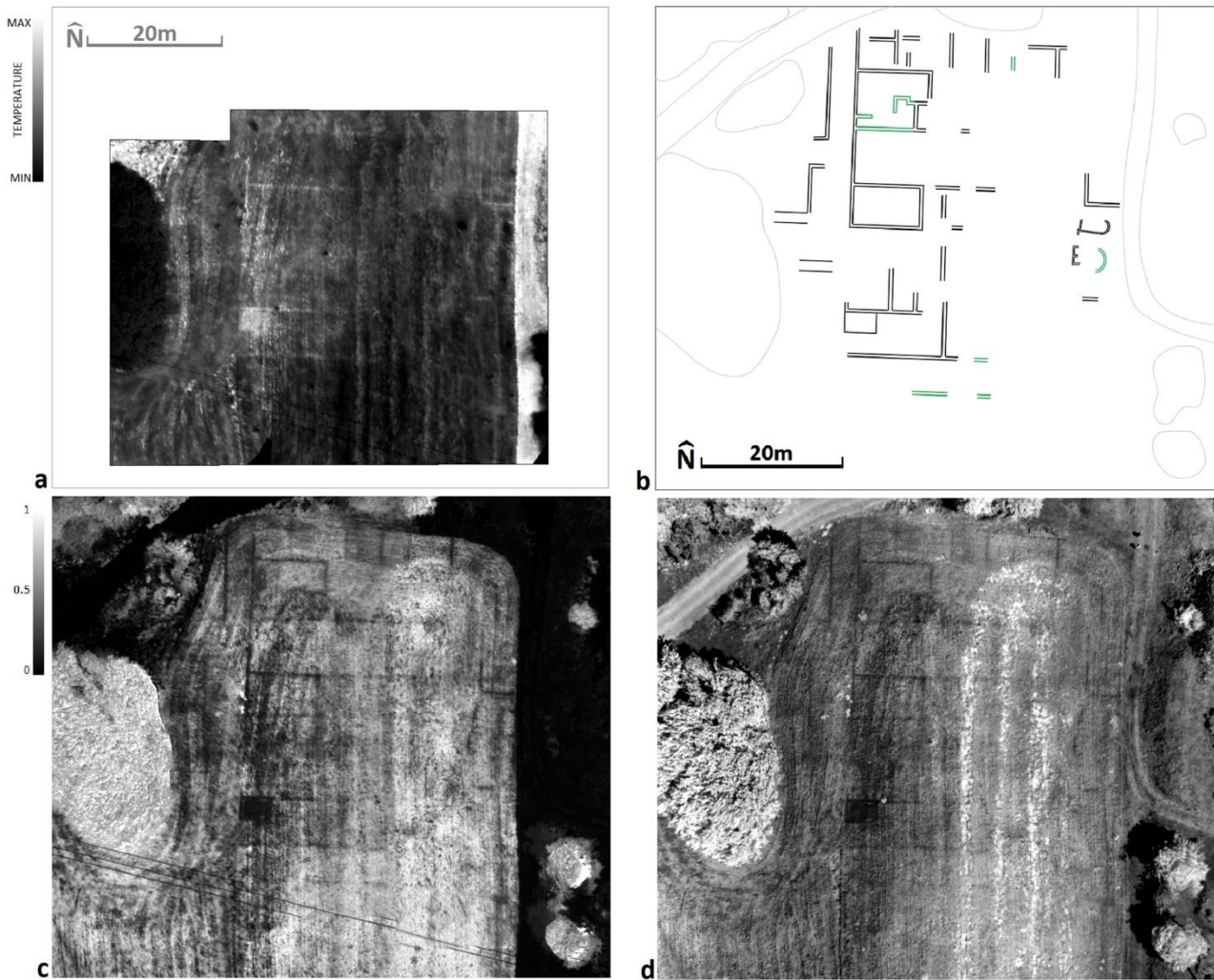
*Figure 10. Philippi, the area included in the yellow frame in Fig. 5; a. The geometrically corrected thermal image; b. The design of the marks found in the images; c. The index map of the SR index for the visual comparison of the observation ability of the marks in relation to the thermal image (a) and the NIR image (d). In the NIR image (d) and even more in the index map of the index SR (c) the crop marks are located optimally, in relation to all the other images collected.*

## 4. DISCUSSION

At the location north of Amphipolis, the observation of crop marks (Fig. 2) was initially allowed in the original satellite image of 2005, as the width of the marks (approximately 40cm, Fig. 4) is sufficient to affect the pixel intensities (60x60cm, Tab. 2) of the satellite image. Negative images (Fig. 2.b; d) help to visually observe the marks.

Aerial photographs of 1945 and 1953 (Fig. 3.a;b) show no marks, as shown in the google earth images of 2010, 2012, 2014 and 2016 (Fig. 3.e-j). However, in the images of google earth of 2017 and 2018 (Fig. 3.k-p) marks are found in a smaller number and with a weak intensity of visual observation. It is certain that the use of the original satellite images (Fig. 2.c-f) allows the optimal observation of the marks in comparison with the same images provided by google earth (Fig. 2.a). This is due to the spatial and quality degradation of the google earth images in relation to the

original satellite images, as well as the absence of the NIR band. However, the intertemporal and repetitive appearance and visual observation of the marks, reinforces the view that, possibly, it is a place with covered ancient architectural remains. Otherwise, that is, in the case of the appearance of marks in one of all available images, it could be stated that their visual observation is due to some random event.

The UAV image of 2019 (Fig. 4) shows the corresponding crop marks of Figs 2 and 3 (linear rendering of the marks in yellow). In addition, places without vegetation are located in the southern part of Fig.4 (yellow arrows), with directions parallel to the sowing direction. This, possibly, means that these marks are not due to underground structures, but some random event. The negative image helps in the visual observation of the marks in this location too. Marks of similar covered structures have been observed in

many other studies (Neubauer et al., 2012; Herrera, 2016; Stewart, 2020).

In the location of Philippi, no image of google earth (Fig. 6) shows marks. This was originally a deterrent to UAV shooting at this location. However, because the location is within the walls of the ancient city, attempts were made to capture images with different sensors.

In the image of the digital DSLR camera (Fig. 8.a) a small number of crop marks with weak intensity are observed, possibly of ancient, covered constructions.

Figure 8.b of the MS sensor clearly shows that the area is covered by a crop. In figure 8.f, ie in the NIR image, the marks of the possible ancient architectural remains are clearly revealed (rendering of black marks in Fig. 10.b). In the other images of the MS sensor (Fig. 8. b-e) the marks are almost absent.

From the vegetation index maps, indexes SR (Fig. 10.c or Fig. 9.f) and GCI (Fig. 9.h) allow, on the one hand, the best visual observation of the existing marks (rendering of black marks in Fig.10.b) of the NIR image (Fig. 10.d or Fig. 8.f) and, on the other hand, the optical observation of additional marks (rendering of marks in green in Fig. 10.b). Marks of similar covered structures have been observed in many other studies (Neubauer et al., 2012; Herrera, 2016; Stewart, 2020). Observations are visually weak on the NDVI, GNDVI, SAVI and GSAVI indexes, and more pronounced on the NLI, NDVIRE, MSR, GRVI, NDRE and NENTI indexes. Some of the above indexes that have been used in similar surveys sometimes lead to good and other times to moderate or bad results (Casella et al., 2018; Agudo et al, 2018; Christopher and Clutterbuck, 2019; Bennett et al., 2012).

There are similar studies in literature where the use of thermal images leads to either positive or moderate results (Uribe et al., 2021; Agudo et al, 2018; Casana et al., 2017; Christopher and Clutterbuck, 2019). In the thermal image (Fig. 10.a), which occupies a smaller space than the images of the other two sensors, the visual intensity is weak and the number of marks is smaller than the detected marks (Fig. 10) in the NIR image and / or in the maps of the SR and GCI indexes.

Lastly, there will be no discussion about the geometric accuracy of the geometric corrections of the images as it is interesting to correlate the images with a relative accuracy and the intensities of visual observation of the marks on the images of different sensors.

## 5. CONCLUSION

Marks of possibly ancient covered ancient architectural remains are found in both study areas. The word "possibly" has been added to the previous sentence, because only archaeological excavation can substantiate the findings of Aerial and Remote Sensing Archaeology.

At the location north of Amphipolis, the intertemporal and repeated appearance and visual observation of the marks (in 2005, 2017, 2018 and 2019), reinforces the view that there are building structures under the ground.

Shots with the UAV and the digital DSLR camera helped in rendering the marks with higher resolution.

In the location of Philippi, although no marks appear in the images of Google Earth, the UAV and digital DSLR camera initially allowed the detection of marks, even in small numbers (marks) and with a weak intensity of visual observation. In this application, the MS sensor is found to be the optimal one, as in its NIR image, the marks of possible ancient architectural remains were clearly and visually revealed. In addition, the use of MS sensor images for the production of vegetation index maps led, on the one hand, to the better visual observation of the marks and, on the other hand, to the observation of additional marks. This was conducted mainly in the images of the SR and GCI indexes.

Unfortunately, in this application the thermal sensor did not give images in which the marks appear in the same or in a greater extent in relation to the NIR image and / or with the above vegetation index maps.

In any case, it is very important that shots are taken within the documented optimal marking period in every study area. Also, the use of UAV and sensors that can be placed on it, which utilize areas of the spectrum beyond the visible range, allow optimal detection and detailed study of marks.

**REFERENCES**

Aasen, H., Honkavaara, E., Lucieer, A. and Zarco-Tejada P.J. (2018) Quantitative Remote Sensing at Ultra-High Resolution with UAV Spectroscopy: A Review of Sensor Technology. Measurement Procedures, and Data Correction Workflows. *Remote Sensing,* Vol. 10, 1091.

Agudo U.P., Pajas A.J., Pérez-Cabello F., Redón V.J. and Lebrón E.B. (2018) The Potential of Drones and Sensors to Enhance Detection of Archaeological Cropmarks: A Comparative Study Between Multi-Spectral and Thermal Imagery. *Drones*, Vol. 2 (29), pp. 1-23.

Ahmed, O.S.; Shemrock, A. Chabot, D., Dillon, C., Williams, G., Wasson, R. and Franklin, S.E. (2017) Hierarchicalland cover and vegetation classification using multispectral data acquired from an unmanned aerial vehicle. *Remote Sensing*, Vol. 38, pp. 2037-2052.

Assmann, J.J., Kerby, T.J., Cunliffe, M.A. and Myers-Smith, H.I. (2019) Vegetation monitoring using multispectral sensors - best practices and lessons learned from high latitudes. *J. Unmanned Veh. Syst.,* Vol. 7, pp. 54-75.

Baladie, R. (1989) *Strabon Geographiae* In Tome IV (Livre VII), Les Belles Lettres: Paris, France, pp. 35-47.

Barnes, E.M., Clarke, T.R., Richards, S.E., Colaizzi, P.D., Haberland, J., Kostrzewski, M., Waller, P., Choi, C., Riley, E., Thompson, T., Lascano, R.J., Li, H. and Moran, M.S. (2000) Coincident detection of crop water stress, nitrogen status and canopy density using ground based multispectral data. *Proceedings of the Fifth International Conference on Precision Agriculture*, Bloomington, Minnesota, USA, 16-19 July 2000, pp. 1-15.

Barrett, G. (1993) Cropmark discoveries in the river barrow valley, Ireland 1989–1991. *J. AARGnews*, Vol. 6, pp. 21-28.

Bennett, R., Welham, K., Hill, R.A. and Ford, A.L.J. (2012) The Application of Vegetation Indices for the Prospection of Archaeological Features in Grass-Dominated Environments. *Archaeological Prospection*, Vol. 19, pp. 209-218.

Berni, A.J., Tejada, P.J.Z., Suárez, L., Dugo, V.G. and Fereres, E. (2009) Remote sensing of vegetation from UAV platforms using lightweight multispectral and thermal imaging sensors. *International Archives of the Photogrammetry, Remote Sensing and Spatial Information Sciences*, Vol. 38, pp. 722-728.

Betti, L.(1963) Le trace nella fotoarcheologia. *Proceedings of the Archéologie Aérienne, Colloque International, SEVPEN*, Paris, France, 31 August - 3 September 1963, pp. 59-75.

Borgogno M.E. and Gajetti, M. (2017) Preliminary considerations about costs and potential market of remote sensing from UAV in the Italian viticulture context. *Eur. J. Remote Sens.,* Vol. 50, pp. 310-319.

Brooks, R.R. and Johannes D. *Phytoarchaeology* Leicester University Press, pp. 135-138.

Candiago, S., Remondino, F., Giglio, M., Dubbini, M. and Gattelli, M. (2015) Evaluating Multispectral Images and Vegetation Indices for Precision Farming Applications from UAV Images. *Remote Sensing*, Vol. 7 (4), pp. 4026-4047.

Casana, J., Wiewel, A., Cool, A., Hill, C.A., Fisher, D.K. and Laugier, J.E. (2017) Archaeological Aerial Thermography in Theory and Practice. *Advances in Archaeological Practice*, Vol. 5 (4), pp. 310-327.

Casella, V., Franzini, M., Gorrini, E.M. (2018). Crop marks detection through optical and multispectral imagery acquired by UAV. *Published in IEEE: Metrology for Archaeology and Cultural Heritage (MetroArchaeo)*, Italy, 22-24 Oct. 2018, pp. pp. 103-118.

Challis, K., Kincey, M. and Howard J.A. (2009) Airborne Remote Sensing of Valley Floor Geoarchaeology using Daedalus ATM and CASI. *Archaeological Prospection,* Vol. 16, pp. 17-33.

Chiang, K.W., Tsai, M.L. and Chu, C.H. (2012) The development of an UAV borne direct georeferenced photogrammetric platform for ground control point free applications. *Sensors*, Vol. 12, pp. 9161-9180.

Ciminale, M., and Ricchetti, E. (1999) Non-destructive exploration in the archaeological park of Metaponto (Southern Italy). *J. Archaeol. Prospect.*, Vol. 6, pp. 75-84.

Christopher, C. and Clutterbuck, B. (2019) Mapping Heterogeneous Buried Archaeological Features Using Multisensor Data from Unmanned Aerial Vehicles. *Remote Sensing*, Vol. 12 (1), pp. 1-31.

Fagan, B. (1959) Cropmarks in antiquity. *Antiquity*, Vol. 33, pp. 279-281.

Franzini, M., Ronchetti, G., Sona, G. and Casella, V. (2019) Geometric and Radiometric Consistency of Parrot Sequoia Multispectral Imagery for Precision Agriculture Applications. *Applied Sciences*, Vol. 9 (5314), pp. 3-24.

Georgoula, O., Kaimaris, D., Karadedos, G. and Patias, P. (2003) Photogrammetry and Archaeology: A case study in the archaeological site of Philippoi in N.Greece. *Proceedings of the CAA (Computer applications*

*and quantitative methods in archaeology) Congress Enter the Past, The E-way into four Dimensions of Cultural Heritage,* City Hall Vienna, Austria, 8-12 April 2003, pp. 409-413.

Gitelson, A.A. and Merzlyak, M.N. (1994) Spectral reflectance changes associated with autumn senescence of Aesculus hippocastanum L. and Acer platanoides L. leaves. Spectral features and relation to chlorophyll estimation. *J. Plant Physiol.,* Vol. 143, pp. 286-292.

Gitelson, A.A., Kaufman, Y.J. and Merzlyak, M.N. (1996) Use of a green channel in remote sensing of global vegetation from EOS-MODIS. *Remote Sens. Environ.,* Vol. 58, pp. 289-298.

Gitelson, A.A., Kaufman, Y.J., Stark, R. and Rundquist, D. (2002) Novel algorithms for remote estimation of vegetation fraction. *Remote Sens. Environ.,* Vol. 80, pp. 76-87.

Godley, D.A. (1921) *Herodotus* Mass Harvard University Press: Cambridge, MA, USA, p. 114.

Goukowsky, P. (1978) *Diodore de Sicile* In Bibliotheque Historiogue Livre XVIII, Lew Belles Lettres: Paris, France, p. 4.

Guo, Y., J. Senthilnath, W. Wu, Zhang, X., Zeng, Z. and Huang. H. (2019) Radiometric Calibration for Multi-spectral Camera of Different Imaging Conditions Mounted on a UAV Platform. *Sustainability*, Vol. 11, 978.

Hanson, W.S. and Olten, A.I. (2003) The identification of roman buildings from the air: recent discoveries in Western Transylvania. *J. Archaeol. Prospect.,* Vol. 10, pp. 101-117.

Hatzopoulos, N.J., Stefanakis, D., Georgopoulos, A., Tapinaki, S., Volonakis, P. and Liritzis, I. (2017) Use of various surveying technologies to 3D digital mapping and modelling of cultural heritage structures for maintenance and restoration purposes: The tholos in Delphi, Greece. *Mediterranean Archaeology and Archaeometry*, Vol. 17 (3), pp. 311-336.

Henrico, I., Combrinck, L. and Eloff. C. (2016) Accuracy comparison of Pléiades satellite ortho-images using GPS device based GCPs against TerraSAR-X-based GCPs. *South African Journal of Geomatics*, Vol. 5 (3), pp. 358-372.

Herrera M.V. (2016) A view from the far west of Europe: Aerial Archaeology at the Merida Institute of Archaeology. *AARGnews*, Vol. 52, pp. 24-33.

Honkavaara, E. and Khoramshahi, E. (2018) Radiometric Correction of Close-Range Spectral Image Blocks Captured Using an Unmanned Aerial Vehicle with a Radiometric Block Adjustment. *Remote Sensing*, Vol. 10, p.256.

Huete, A.R. (1988) A soil-adjusted vegetation index (SAVI). *Remote Sensing of Environment*, Vol. 25 (3), pp. 295-309.

Hunt, E.R., Cavigelli, M., Daughtry, C.S.T., McMurtrey, J.E. and Walthall, C.L. (2005) Evaluation of digital photography from model aircraft for remote sensing of crop biomass and nitrogen status. *Precision Agriculture*, Vol. 6, pp. 359-378.

Johansen, K. and Raharjo, T. (2017) Multi-temporal assessment of lychee tree crop structure using multi-spectralRPAS imagery. *Int. Arch. Photogramm. Remote Sens. Spatial Inf. Sci.,* Vol. 42, pp. 165-170.

Jones, S.H. (1970) *Thucydidis: Historiae Tomus Posterior, OXONII* E Typographeo Clarendonioano, Reprindet, Clarendon: Oxford, UK, pp. 100-108.

Jones, R. J. A. and Evans, R. (1975) Soil and crop marks in the recognition of archaeological sites by air photography. *Aerial Reconnaissance for Archaeology*, Vol. 12, pp. 1-11.

Kaimaris, D. (2002) *Photogrammetry-Photointerpretation: Research tools in Archaeology* Master Thesis, Aristotle University of Thessaloniki, Thessaloniki, Greece.

Kaimaris, D. (2006) *Photogrammetric processing of digital images in the service of archaeological research: the localization of Via Egnatia from Amphipolis to Philippi* Ph.D. Thesis, Aristotle University of Thessaloniki, Thessaloniki, Greece.

Kaimaris, D., Georgoula, O., Patias, P., Stylianidis, E. (2011) Comparative analysis on the archaeological content of imagery from Google Earth. *Journal of Cultural Heritage*, Vol. 12 (3), pp. 263-269.

Kaimaris, D., Patias, P. and Tsakiri, M. (2012) Best period for high spatial resolution satellite images for the detection of marks of buried structures. *The Egyptian Journal of Remote Sensing and Space Sciences*, Vol. 15 (1), pp. 9-18.

Kaimaris, D. and Patias, P. (2015) Systematic observation of the change of marks of known buried archaeological structures: Case study in the plain of Philippi, Eastern Macedonia, Greece. *Mediterranean Archaeology and Archaeometry*, Vol. 15 (2), pp. 129-142.

Kaimaris, D., Patias, P., Georgoula, O. and Karadedos, G. (2016) *First thoughts about the location of the potential roads of Nine Roads (Amphipolis) with geoinformation tools* Honorary Book for Emeritus Professor Ch. Kaltsikis, Ziti: Thessaloniki, Greece, pp. 239-251.

Kaimaris, D., Karadedos, G., Georgiadis, Ch., Patias P. (2018a) Locating and Mapping the Traces of the Covered Ancient Theater of Amphipolis (Eastern Macedonia, Greece). *Heritage*, Vol. 1 (2), pp. 306-319.

Kaimaris, D (2018b) Ancient theaters in Greece and the contribution of geoinformatics to their macroscopic constructional features. *Scientific Culture,* Vol. 4 (3), pp. 9-25

Kaimaris, D., Patias, P., Mallinis, G. and Georgiadis, Ch. (2019) Data Fusion of Scanned Black and White Aerial Photographs with Multispectral Satellite Images. *Journal Science,* Vol. 1 (36), pp. 1-13.

Krishnana, S., Sajikumar, N. and Sumam, K. (2016) DEM Generation Using Cartosat-I Stereo Data and its Comparison with Publically Available DEM. *Procedia Technology*, Vol. 24, pp. 295-302.

Lazaridis, D.1993. *Amphipolis* Ministry of Culture: Athens, Greece, pp. 15-137.

Liritzis, I., Al-Otaibi, F.M., Volonakis, P. and Drivaliari, A. (2015) Digital technologies and trends in cultural heritage. *Mediterranean Archaeology and Archaeometry*, Vol. 15 (3), pp. 313-332.

Lussem, U., Bareth, G., Bolten, A. and Schellberg., J. (2017) Feasibility study of directly georeferenced images from low-cost unmanned aerial vehicles for monitoring sward height in a long-term experiment on grassland. *Grassl. Sci. Eur.*, Vol. 22, pp. 354-356.

Mafanya, M., Tsele, P., Botai, J.O., Manyama, P., Chirima, G.J. and Monate, T. (2018) Radiometric calibration framework for ultra-high-resolution UAV-derived orthomosaics for large-scale mapping of invasive alien plants in semi-arid woodlands: Harrisia pomanensis as a case study. *Int. J. Remote Sens.*, Vol. 39, pp. 5119-5140.

Miyoshi, G.T., Imai, N.N., Tommaselli, A.M.G., Honkavaara, E., Näsi, R. and Moriya, E.A.S. (2018) Radiometric block adjustment of hyperspectral image blocks in the Brazilian environment. *Int. J. Remote Sens.*, Vol. 39, pp. 4910-4930.

Moriarty, Ch., Cowley, C.D., Wade, T., Nichol, J.C. (2018) Deploying multispectral remote sensing for multitemporal analysis of archaeological crop stress at Ravenshall, Fife, Scotland. *Archaeological Prospection*, pp. 1-14.

National Cadaster (2021) Available online: http://gis.ktimanet.gr/wms/apr1/ (Accessed on 17 November 2021).

Neubauer W., Doneus M., Trinks I., Verhoeven G., Hinterleitner A., Seren S. and Löcker K. (2012) *Long-term Integrated Archaeological Prospection at the Roman Town of Carnuntum/Austria. Archaeological survey and the city* Publisher: Oxbow Books, Editors: Johnson Paul, Millet Martin, pp.202-221.

Peter, G.B., Messina, P.J., Carroll, W.J., Zhi, J., Chimonyo, V., Lin, S. and Snapp. S. (2020) Multi-Spatial Resolution Satellite and sUAS Imagery for Precision Agriculture on Smallholder Farms in Malawi. *Photogrammetric Engineering and Remote Sensing*, Vol. 86 (2), pp. 107-119.

Rouse, J.W., Haas, R.H., Schell, J.A. and Deering, D.W. (1974) Monitoring Vegetation System in the Great Plains with ERTS. *Proceedings of the Third Earth Resources Technology Satellite-1 Symposium*, Greenbelt, MD, USA, 10-14 December 1974.

Skycat (2014) *Skycat Brochure* Available online:
https://static1.squarespace.com/static/53428f61e4b0cc3fc1bc3f80/t/56385284e4b0936ed2c45bfd/144653171 6039/Skycat+handout.pdf (Accessed on 17 November 2021).

Stewart, C., Labrèche, G., González, L.D. (2020) A Pilot Study on Remote Sensing and Citizen Science for Archaeological Prospection. *Remote Sensing*, Vol. 12 (17) 2795, pp. 1-16.

Turner, D., Lucieer, A. and Watson, C. (2012) An automated technique for generating georectified mosaics from ultrahigh resolution unmanned aerial vehicle (UAV) imagery, based on structure from motion (SfM) point clouds. *Remote Sensing,* Vol. 4, pp. 1392-1410.

Uribe, P., Angás, J., Romeo, F., Pérez-Cabello, F. and Santamaría, D. (2021) Mapping Ancient Battlefields in a multi-scalar approach combining Drone Imagery and Geophysical Surveys: The Roman siege of the oppidum of Cabezo de Alcalá (Azaila, Spain). *Journal of Cultural Heritage,* Vol. 48, pp. 11-23.

Wilson, D.R. (1982) *Air Photo Interpretation for Archaeologists* Batsford, London, pp. 50-55.